RSC Advances

PAPER

View Article Online
View Journal | View Issue

Cite this: *RSC Adv.*, 2023, **13**, 23308

Prolonged release of an antimicrobial peptide GL13K-loaded thermosensitive hydrogel on a titanium surface improves its antibacterial and anti-inflammatory properties†

Lin Zhou,‡[ab] Yifeng Xing,‡[bc] Yanjin Ou,‡[ac] Jiamin Ding,[d] Yu Han,[e] Dong Lin[a] and Jiang Chen *[ab]

The application of titanium in the orthopedic and dental fields is associated with bacterial infection and chronic inflammation, especially in the early stages after its implantation. In the present study, we investigated the antibacterial and anti-inflammatory activities of a titanium surface that was immobilized in a thermosensitive PLGA-PEG-PLGA hydrogel containing the antimicrobial peptide GL13K. The FTIR results confirmed the successful loading of GL13K. The degradation of the hydrogel and release of GL13K persisted for two weeks. The modified titanium surface exhibited a significant inhibitory effect on *Porphyromonas gingivalis* in contact with its surface, as well as an inhibitory effect on *P.g* in the surrounding environment by releasing GL13K antimicrobial peptides. The modified titanium surfaces were biocompatible with RAW264.7. Furthermore, the expression of pro-inflammatory cytokines IL-1β, TNF-α and iNOS was down-regulated, whereas anti-inflammatory cytokines Arg-1, IL-10 and VEGF-A were up-regulated on the modified titanium surfaces on days 3 and 5. This effect was attributed to the polarization of macrophages from the M1 to M2 phenotype, which was confirmed by the detection of macrophage M1/M2 biomarkers *via* immunofluorescence staining and flow cytometry. Thus, the thermosensitive PLGA-PEG-PLGA hydrogel release system carrying the antimicrobial peptide GL13K on a titanium surface exhibited antibacterial and anti-inflammatory properties and promoted macrophage polarization from the M1 to M2 phenotype, which may help create a favourable niche for bone formation under infective condition.

Received 22nd May 2023
Accepted 17th July 2023

DOI: 10.1039/d3ra03414c

rsc.li/rsc-advances

1 Introduction

Presently, titanium nails and plates are used in orthopedics and dental implantation to replace tissue damaged by various diseases.[1,2] However, besides the risk of bacterial or fungal infections in the implant area, these implants usually exhibit a specific foreign body response (FBR), which is associated with inflammation.[3]

Blood clot is adsorbed on the surface of implants after implantation, leading to the formation of a temporary matrix around the implants.[4] The temporary matrix contains abundant growth factors, cytokines and chemical agents, which recruit cells such as macrophages and monocytes from the immune system to the damaged area. The recruited cells secrete numerous inflammatory mediators, such as leukocyte-1β (IL-1β), leukocyte-6 (IL-6), and tumor necrosis factor-α (TNF-α), resulting in acute inflammation.[5] Macrophages are innate immune cells, which first colonize the surface of the implant, undergo inflammatory chemotaxis, migrate to the injured site, and lead the body's defense against foreign bodies. Macrophages can be divided into M1 and M2 biotypes.[6] An abundance of M1 macrophages in the implant area leads to persistent inflammation and interferes with the healing process. In contrast, an abundance of M2 macrophages in the implant facilitates anti-inflammatory and regenerative mechanisms.[7,8] Immune inflammatory responses including macrophage polarization occur in 1 to 14 days, followed by initiation of regeneration during osseointegration.[9] Therefore, the antibacterial and anti-inflammatory properties of the implant surface play an important role in healing, especially during the

[a]*Affiliated Stomatological Hospital of Fujian Medical University, Fujian Medical University Fujian, China. E-mail: jiangchen@fjmu.edu.cn*

[b]*Fujian Key Laboratory of Oral Diseases, School and Hospital of Stomatology, Fujian Medical University, Fuzhou, China*

[c]*Fujian Biological Materials Engineering and Technology Center of Stomatology, Fujian Medical University, Fuzhou, China*

[d]*Department of Oral Mucosa, Affiliated Stomatological Hospital of Fujian Medical University, Fuzhou, China*

[e]*Division of Craniofacial Development and Tissue Biology, Graduate School of Dentistry, Tohoku University, Sendai City, Japan*

† Electronic supplementary information (ESI) available. See DOI: https://doi.org/10.1039/d3ra03414c

‡ These authors contributed equally to this work.

early stage. Furthermore, reducing inflammation and promoting the polarization of macrophages to the M2 biotype at an early stage are important for healing. The anti-bacterial and anti-inflammatory properties of biomaterials are closely related, resulting in the transformation of 'immunomodulatory biomaterials' to 'immunomodulatory antimicrobial biomaterials'.

Different from general implants, the mouth is a bacterial environment, and thus there is a risk of bacterial colonization of dental implants. Therefore, biofilm formation on implant surfaces induced by bacterial infection is a major concern in implant failure.[10,11] Bacterial infections associated with dental implants, including *Porphyromonas gingivalis* and *Streptococcus mutans*, involve periodontal tissue and dental pulp inflammation. The early adhesion of bacteria is critical to biofilm formation. The most effective method to eliminate or reduce biofilm formation involves the inhibition of bacterial proliferation at an early stage especially within 2 weeks.[12] The formation of a microbial biofilm on the titanium surface further activates the host immune response, resulting in a chronic and aggravated inflammatory response and implant failure.[13] Preventing early bacterial adhesion is important for the formation of transmucosal seal.

The antimicrobial peptide (AMP) GL13K is a short-chain oligopeptide consisting of 14 amino acids. Our previous research demonstrated that GL13K exhibited antibacterial and anti-inflammatory activity.[14,15] However, the biological coating of the implant had insufficient binding force and it easily fell off, which limits its use. Meanwhile, hydrogels possess 3D structures, making them ideal drug delivery system. They are excellent extracellular matrix (ECM) analogs with strong hydration and biocompatibility.[16,17] The polylactide-glycolide/polyethylene glycol/polylactide-glycolide triblock copolymer (poly(D,L-lactide-*co*-glycolide)-poly(ethylene glycol)-poly(D,L-lactide-co-glycolide) (PLGA-PEG-PLGA)) thermosensitive hydrogel shows injectability, biodegradability and biocompatibility. Furthermore, this type of hydrogel not only exhibits degradation and absorption characteristics, it undergoes a reversible sol–gel transition with temperature changes, from a liquid sol at low temperature to a solid gel when the temperature is increased (adjustable to body temperature).[18,19] A thermosensitive hydrogel containing GL13K was injected around the neck of an implant or abutment in the case of local infection or inflammation. The hydrogel adhered to the titanium surface *via* dopamine. The prolonged release of the antibacterial peptide GL13K led to longer antibacterial and anti-inflammatory effects. Thus, a fixed, long-lasting antibacterial and anti-inflammatory microenvironment could be formed around the implant or abutment to treat or prevent infection and inflammatory reactions.

In this study, we used the commercially available PLGA-PEG-PLGA thermosensitive hydrogel to load the antimicrobial peptide GL13K for its prolonged release on titanium surfaces. The objective was to establish a prolonged release system on a titanium surface to induce antibacterial and anti-inflammatory effects, followed by macrophage polarization to the M2 biotype.

2 Results

2.1 Characterization of modified titanium surfaces

2.1.1 Macro form of modified thermosensitive hydrogel and titanium samples. The GL13K-loaded thermosensitive

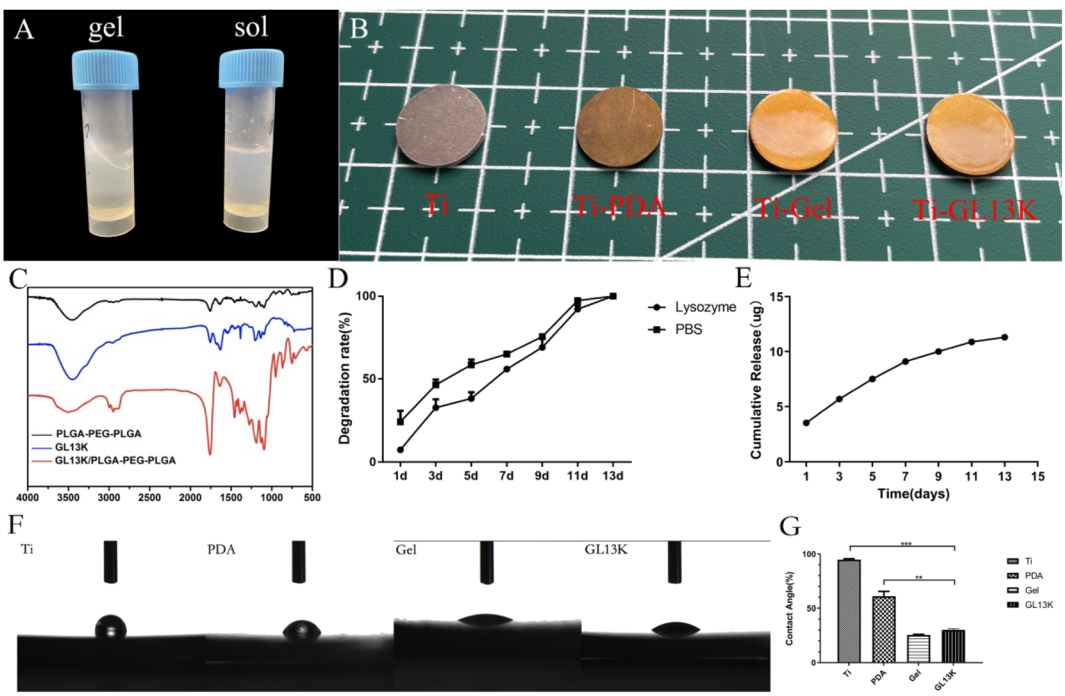

Fig. 1 Characterization of the modified titanium surfaces. (A) Sol and gel phases of the GL13K-loaded thermosensitive hydrogel. (B) Macro form of different modified titanium surfaces. (C) Results of FTIR. (D) Degradation of Ti-GL13K surfaces *in vitro*. (E) GL13K release of the Ti-GL13K surfaces *in vitro*. (F) Water contact angle of different modified titanium surface. (G) Statistical graph of water contact angle.

hydrogel was prepared and its temperature-sensitive sol–gel phase transition behavior is illustrated in Fig. 1A. The temperature-sensitive hydrogel containing the antimicrobial peptide GL13K behaved as a liquid sol at a temperature lower than its transformation temperature and solid gel at temperatures higher than its transformation temperature. As shown in Fig. 1B, a thin layer of hydrogel appeared on the surface of the Ti-Gel and Ti-GL13K samples.

2.1.2 Identity of the functional groups of the composite. The hydrogel and GL13K mixture was monitored *via* FTIR. The absorption bands at 1458 cm^{-1} and 1758 cm^{-1} are attributed to the methyl and carbonyl groups, respectively. The intensity of the peaks in the spectrum of the mixture was stronger than that at 1458 cm^{-1} and the 1758 cm^{-1}, which suggests that the number of methyl and carbonyl groups in the mixture was higher than the hydrogel and GL13K alone. The FTIR results shown in Fig. 1C confirm the successful loading of the GL13K antimicrobial peptide.

2.1.3 Wettability of different modified samples. The water contact angle and results of the quantitative analysis are presented in Fig. 1F and G, respectively. The water contact angles of Ti, Ti-PDA, Ti-Gel and Ti-GL13K were (94.76 ± 1.05)°, (60.92 ± 5.78)°, (25.56 ± 0.69)° and (30.29 ± 1.24)°, respectively. The water contact angles of the Ti-Gel and Ti-GL13K samples were significantly lower than that of the Ti and Ti-PDA samples.

2.1.4 Degradation of the hydrogel. The degradation of the hydrogel coating persisted for nearly 2 weeks, as shown in Fig. 1D. The degradation rate in the early stage was faster than in the later stage. The degradation rate in PBS appeared to be slightly higher than that in lysozyme.

2.1.5 GL13K release. The calibration curve of GL13K is presented in ESI Fig. 1.† As shown in Fig. 1E, the release of the GL13K antimicrobial peptide persisted for 2 weeks. The release in the first week was greater than in the second week and decreased eventually.

2.2 *In vitro* antibacterial assay

2.2.1 Contact antibacterial capacity. The different titanium samples were immersed in a *P. gingivalis* suspension to measure their contact antibacterial capacity. As shown in Fig. 2A, the OD value of the Ti-GL13K titanium group was (0.143 ± 0.004), (0.176 ± 0.016) and (0.166 ± 0.010) at 24 h, 48 h and 72 h, which was significantly lower than that of Ti group with values of (0.730 ± 0.029), (0.879 ± 0.053) and (0.933 ± 0.039), respectively. The colony number of the Ti-GL13K titanium groups was (9.67 ± 1.70), (25.67 ± 1.89) and (37 ± 6.16), which was significantly lower than that of the other three groups. The CFU results are consistent with the OD results, as shown in Fig. 2B. The results of live/dead staining (Fig. 2C) showed that the microbial biofilms were stained in green on the Ti, Ti-PDA and Ti-Gel titanium surfaces, while only a few live bacteria on the Ti-GL13K titanium surface was stained green in 72 h.

2.2.2 The release antibacterial capacity. The release antibacterial capacity was measured by adding a *P. gingivalis* suspension to the extraction medium of the different titanium surfaces. As shown in Fig. 3A, the OD value of the Ti-GL13K titanium groups was (0.148 ± 0.004), (0.139 ± 0.001) and (0.134 ± 0.001) on days 1, 3 and 5, which was significantly lower than that of the Ti group with values of (0.307 ± 0.004), (0.296 ± 0.005) and (0.314 ± 0.007), respectively. Meanwhile, the OD values of the Ti

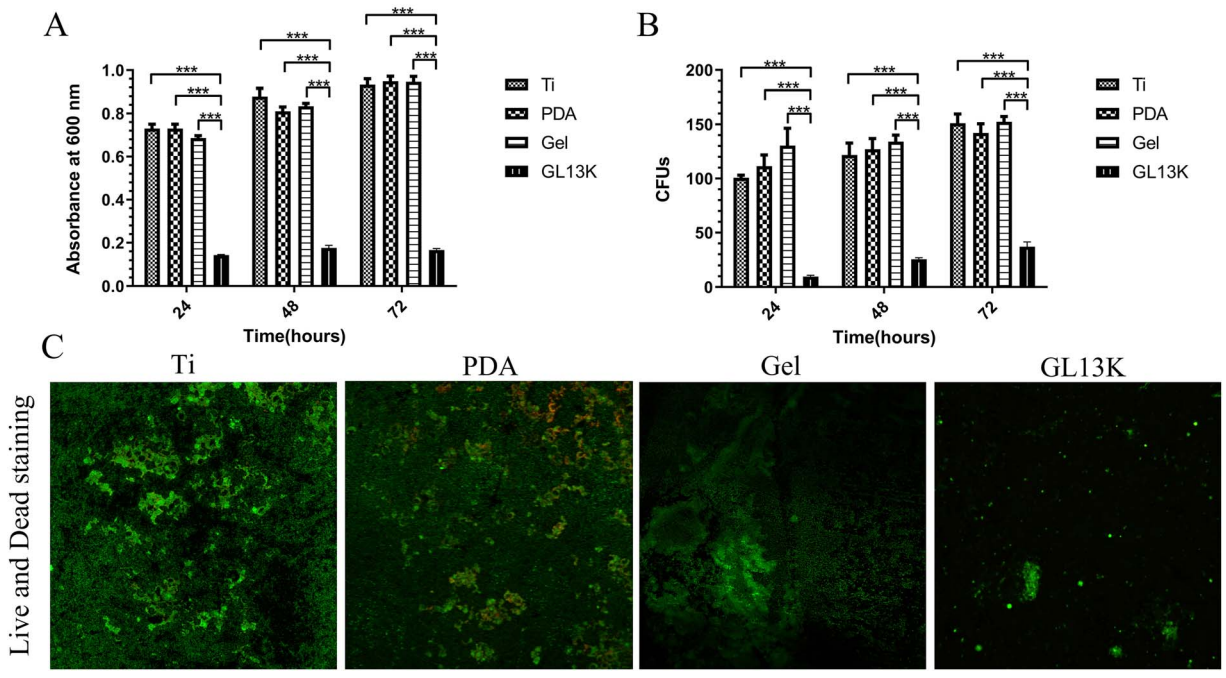

Fig. 2 Contact antibacterial capacity. Antibacterial activity of the different titanium surfaces against *P. gingivalis* in 24 h, 48 h, and 72 h, including OD value of bacterial proliferation (A) and CFU tests (B). (C) Live and dead staining of the adhered bacteria. Error bars represent mean ± SD for $n = 5$, ***$p < 0.001$.

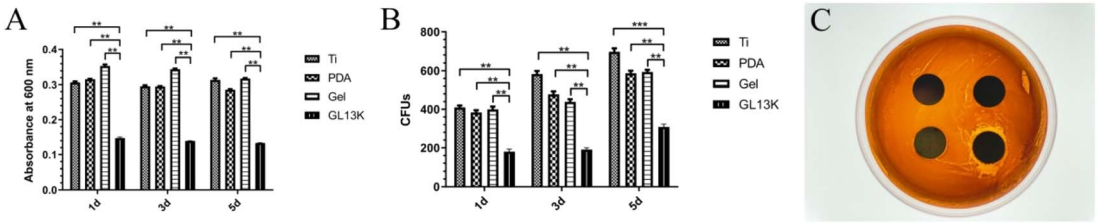

Fig. 3 Release antibacterial capacity. The antibacterial activity of different extraction media against *P. gingivalis* after 24 h, 48 h, and 72 h, including OD value of bacterial proliferation (A) and CFUs (B). (C) Bacteriostatic circles of the different titanium surfaces. Error bars represent mean ± SD for $n = 5$, $^{**}p < 0.05$, and $^{***}p < 0.001$.

group and other two groups were similar. The CFUs are consistent with the OD results, as shown in Fig. 3B. Meanwhile, the results of bacteriostasis in Fig. 3C showed an obvious inhibition zone around the Ti-GL13K titanium sample. The bacteriostatic circle was evenly formed around the sample.

2.3 Biocompatibility assays

2.3.1 Protein adsorption. The BCA protein assay kit was used to observe the protein adsorption. As shown in Fig. 4C, the protein concentrations on Ti-PDA were (0.339 ± 0.008) and (0.257 ± 0.002), Ti-Gel were (0.346 ± 0.009) and (0.412 ± 0.007), and Ti-GL13K were (0.334 ± 0.005) and (0.314 ± 0.002) at 2 and 4 h, which were higher than that on the Ti surface (0.105 ± 0.0008 and 0.140 ± 0.001 at 2 and 4 h), indicating that the three groups improved the adsorption capacity of protein, respectively. Among them, the Ti-Gel titanium surface group showed the optimal protein adsorption, even higher than that of the Ti-GL13K titanium surface.

2.3.2 Cell adhesion. DAPI fluorescence staining was used to observe the macrophage attachment on the different modified titanium surfaces at 2, 4 and 6 h. The attached macrophages on the different titanium surfaces increased with an increase in the culture time, as shown in Fig. 4A. The number of attached cells was (208.0 ± 23.0), (277.7 ± 22.4) and (478.3 ± 20.9) on the Ti group, (245.7 ± 10.3), (197.3 ± 19.2) and (507.0 ± 23.0) on the Ti-PDA group, (243.3 ± 19.2), (395.3 ± 23.9) and (702.7 ± 12.9) on the Ti-Gel group, and (284.3 ± 12.7), (424.7 ± 24.1) and (748.3 ± 31.3) on the Ti-GL13K group at 2,4 and 6 h, respectively. The results of the quantitative analysis presented in Fig. 4B revealed no statistically significant differences among the groups at 2 h. However, the number of macrophages attached on the Ti-Gel and Ti-GL13K titanium surfaces was significantly higher than in the Ti and Ti-PDA group at 4 and 6 h. Further, there was no statistically significant difference between the Ti-Gel and Ti-GL13K titanium surfaces at the three time periods.

2.3.3 Cell proliferation. The CCK-8 assay was used to measure the macrophage proliferation on the different modified titanium surfaces at 12, 24, 72, 120 and 168 h. As shown in Fig. 4D, the OD values of the different modified titanium surfaces were almost the same. No statistically significant differences were detected among the Ti, Ti-Gel and Ti-GL13K titanium surfaces. However, the cell proliferation of Ti-PDA at 72 h and 120 h was lower than on the other titanium surfaces. The CCK-8 results revealed no toxicity of the hydrogel and the mixture of hydrogel and GL13K, which did not improve the cell proliferation.

2.4 Macrophage polarization

2.4.1 Cytokine secretion. The secretion of inflammatory and anti-inflammatory cytokines in the different groups on days 3 and 5 was measured by ELISA. As shown in Fig. 5, the secretion of the pro-inflammatory cytokines IL-1β, TNF-α, and iNOS in the Ti-GL13K titanium surfaces was down-regulated on days 3 and 5 compared with the other groups, except that no statistically significant differences were found between the Ti-Gel and Ti-GL13K titanium surfaces in IL-1β and iNOS on day 5. However, the levels of the anti-inflammatory cytokines Arg-1, IL-10 and VEGF-A secreted on the Ti-GL13K titanium surfaces were up-regulated on days 3 and 5 compared with the other groups. However, no statistically significant differences in Arg-1 were detected among the different titanium surfaces on day 5.

2.4.2 Gene expression. The gene expression of inflammatory and anti-inflammatory cytokines in the different groups on days 3 and 5 was measured by qRT-PCR. As shown in Fig. 6, the relative mRNA levels of IL-1β on day 5 and that of TNF-α and iNOS on day 3 were significantly decreased in the Ti-GL13K titanium surface compared with the other groups. The levels of IL-1β on day 3 and TNF-α on day 5 showed no significant difference among the groups. However, the relative mRNA levels of Arg-1, IL-10 and VEGF-A in the Ti-GL13K titanium surface significantly increased compared with the control Ti group on days 3 and 5.

2.4.3 Immunofluorescence staining. The M1 macrophage markers iNOS and M2 macrophage marker CD163 on the different titanium surfaces were detected *via* immunofluorescence staining. As shown in Fig. 7A and B, the expression of iNOS on the Ti-GL13K titanium surface was less compared with the other groups. The semi-quantitative analysis revealed that the iNOS fluorescence intensity of RAW264.7 cells on the Ti-GL13K titanium surface was significantly lower than that in the other groups compared with the optimal intensity in the Ti and Ti-PDA groups. However, the expression of CD163 on the Ti-GL13K titanium surface was the strongest among the groups. The semi-quantitative analysis also showed that the CD163 fluorescence intensity of the RAW264.7 cells on the Ti-GL13K titanium surface was significantly higher than in the other groups.

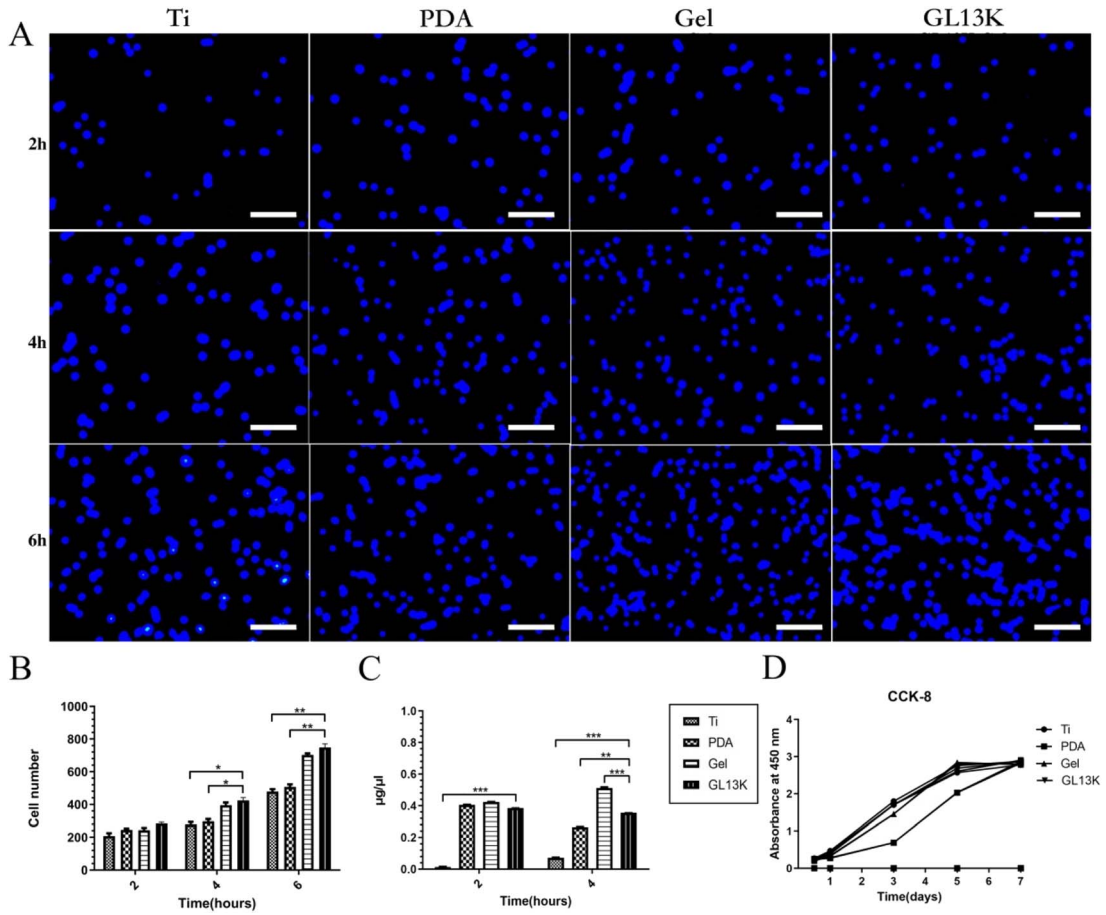

Fig. 4 Biocompatibility of different modified titanium surfaces. (A) Initial adhesion of RAW264.7 cells to different surfaces at 2 h, 4 h, and 6 h. The cell nucleus was stained by DAPI (blue signals). (B) Number of adhered cells on the different surfaces. (C) Protein adsorption on different titanium surfaces. (D) OD values of proliferated RAW264.7 cells on different samples cultured for 12 h, 24 h, 3 d, 5 d, and 7 d. Error bars represent mean ± SD for $n = 5$, $^{*}p < 0.01$, $^{**}p < 0.05$, and $^{***}p < 0.001$.

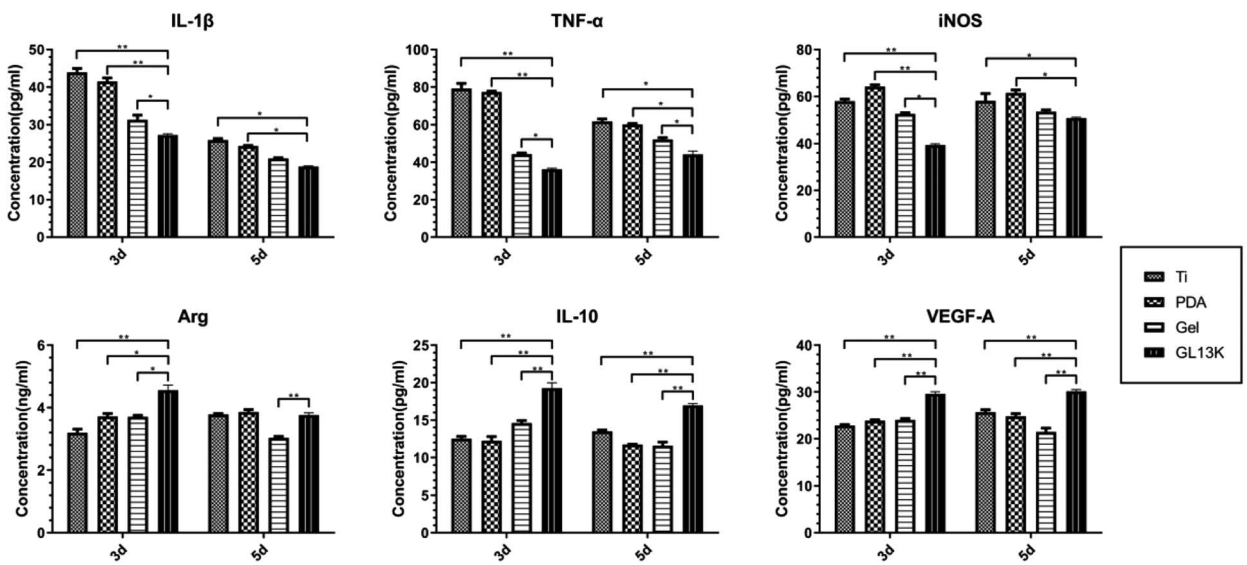

Fig. 5 ELISA of pro-inflammatory cytokines IL-1β, TNF-α and iNOS, and the anti-inflammatory cytokines Arg-1, IL-10 and VEGF-A cultured on different titanium surfaces at 3 and 5 days. Error bars represent mean ± SD for $n = 5$, $^{*}p < 0.01$, and $^{**}p < 0.05$.

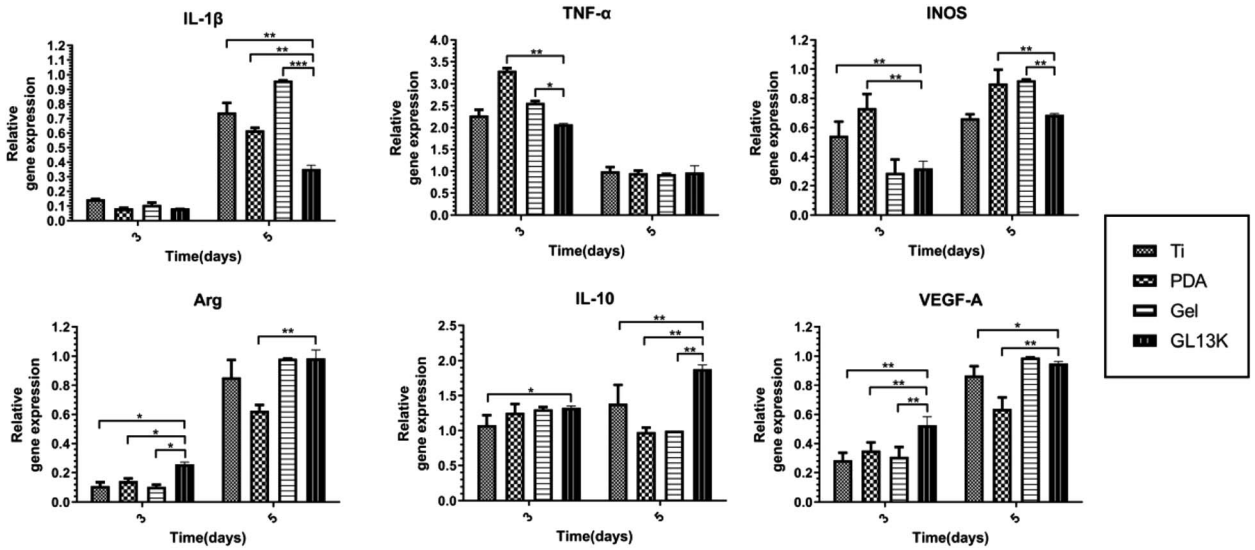

Fig. 6 Gene expression of the pro-inflammatory cytokines IL-1β, TNF-α and iNOS, and anti-inflammatory cytokines Arg-1, IL-10 and VEGF-A cultured on the different titanium surfaces at 3 and 5 days. Error bars represent mean ± SD for $n = 5$, *$p < 0.01$, **$p < 0.05$, and ***$p < 0.001$.

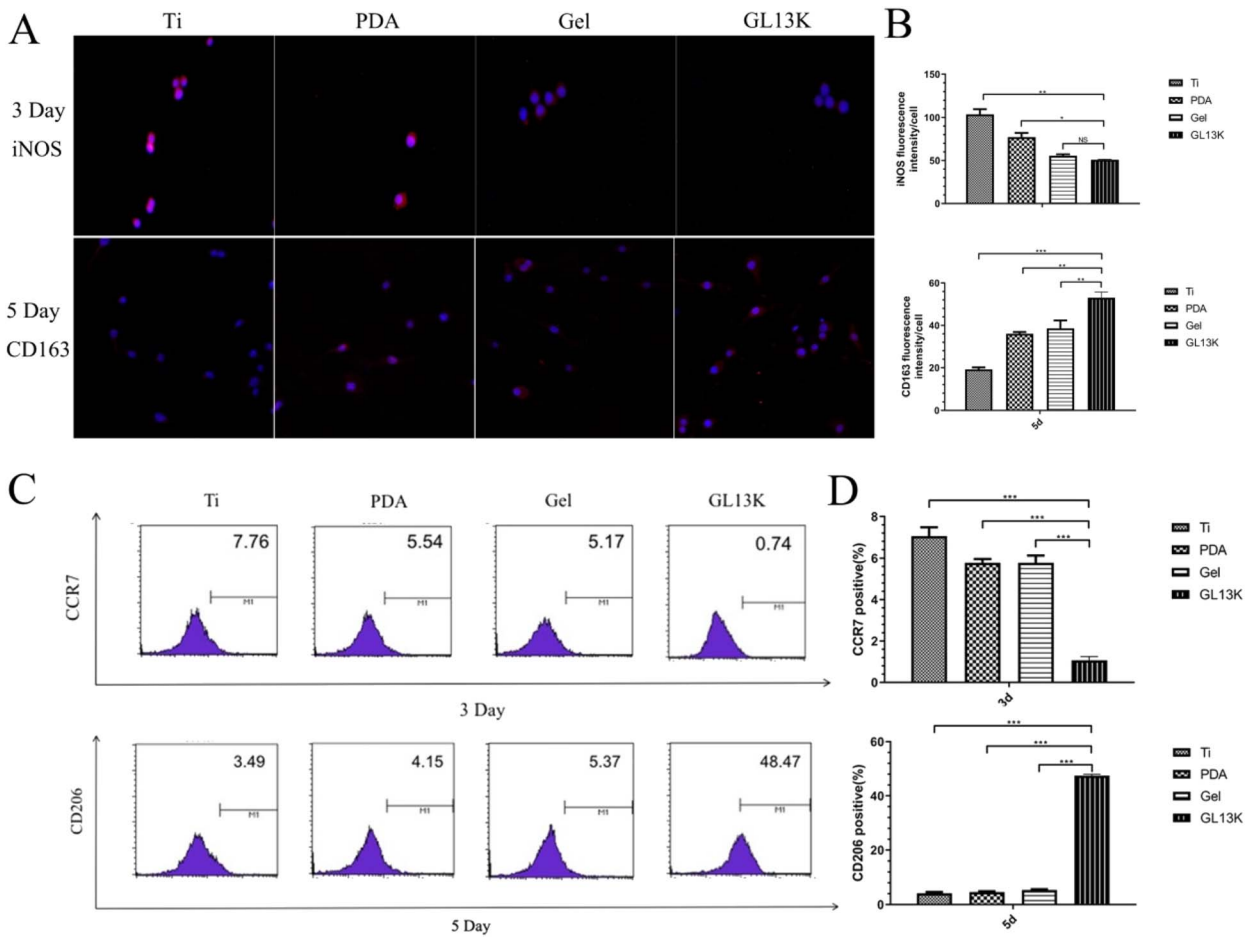

Fig. 7 Polarization of macrophages on different titanium surfaces. (A) Immunofluorescence staining of M1 macrophage markers iNOS (red signals) at 3 days and M2 macrophage markers CD163 (red signals) at 5 days on different titanium surfaces. (B) Fluorescence intensity of iNOS and CD163. (C) Flow cytometry analysis of M1 and M2 macrophage surface markers CCR7 and CD206. (D) Percentage of CCR7 (M1) and CD206 (M2) determined by flow cytometry. Error bars represent mean ± SD for $n = 5$, *$p < 0.01$, **$p < 0.05$, and ***$p < 0.001$.

2.4.4 Flow cytometry. Other macrophage surface markers CCR7 (M1) and CD206 (M2) were measured by flow cytometry. Fewer cells on the Ti-GL13K titanium surface exhibited the M1 macrophage surface marker CCR7 by day 3, as shown in Fig. 7C and D. The results showed a significant difference. Meanwhile, the cells on the Ti-GL13K titanium surface exhibited an additional M2 macrophage surface marker CD206 compared with the other groups by day 5.

3 Discussion

Early bacterial adhesion and inflammatory reaction after implant placement affect osseointegration and are the main influencing factors of early implant failure.[20,21] Therefore, the inhibition of bacterial adhesion and reduction of inflammation at an early stage is important for osseointegration. The antibacterial and anti-inflammatory role of the antimicrobial peptide GL13K has been studied in recent years.[15,22] In this study, AMP GL13K was continuously released from the titanium surface for two weeks by a thermosensitive hydrogel, resulting in early antibacterial and anti-inflammatory effects.

Some studies reported that the surrounding environment was in an inflammatory phase 7 days after implant placement, and osteogenesis occurred mainly on days 7 to 14 of healing.[9] Thus, the formation of a plaque biofilm was prevented and the inflammatory response was reduced before 7 days of healing, which is extremely important for successful implantation. In the present study, a thermosensitive hydrogel containing AMP GL13K on a titanium surface was successfully fabricated, which was hydrophilic based on the FTIR and GL13K release assay results. The increasing numbers of methyl and carbonyl group confirmed the successful combination of the hydrogel and GL13K. GL13K release was accompanied by the degradation of the hydrogel, which persisted for almost two weeks. As reported by Jing *et al.*, the residual mass of the PLGA-PEG-PLGA hydrogels (20 wt%) on a scaffold on day 15 was less than 10%,[23] which is consistent with our results.

The antibacterial assays demonstrated that the titanium surface exhibited both antibacterial contact and release. *P. gingivalis* is the main bacterial pathogen in peri-implantitis and the main oral bacteria.[24] In the present study, the Ti-GL13K titanium surface effectively inhibited the proliferation of *P. gingivalis* and prevented the formation of bacterial biofilms by releasing GL13K continually. The released GL13K interacted with the bacterial membranes, resulting in bacterial death. The bacterial membranes are negatively-charged,[25] while AMP GL13K is positively charged,[26] resulting in electrostatic attraction and interaction.[27] Models such as the barrel-stave model and toroidal-pore model demonstrated that bacteria membrane disruption is the major mechanism for the death of bacteria.[27–29] Bacterial cell death induced by antimicrobial peptides prevents drug resistance to other antibacterial agents such as antibiotics. Li *et al.* reported that AMP GL13K exhibited antibacterial activity against methicillin-resistant *Staphylococcus aureus* (MRSA).[22] Further, the release of GL13K prevented the formation of a microbial biofilm, which was a major factor leading to the failure of osseointegration. Microbial biofilms are highly structured matrix-enclosing sessile bacterial communities, which hinder bacterial eradication.[30] The Ti-GL13K titanium surface prevented the adhesion of *P. gingivalis*. As shown in Fig. 2C, it released GL13K, which acted as a bactericide. However, the roughness and hydrophilicity of the material surface affect the early adhesion of the bacteria.[31,32] Bacteria attached to the Ti-GL13K titanium surface with good hydrophilicity. However, the experimental results contradict the theoretical findings, which may be related to the material properties, surface appendages and bacterial species.[33] Nonetheless, the continuous release of GL13K from the surface of the thermosensitive hydrogel titanium decreased the number of bacteria around the titanium surface. Therefore, we speculated that this may also decrease the number of bacteria attached to the surface of the hydrogel titanium.

Implantation triggers protein adsorption around the biomaterial, followed by colonization and proliferation of immune cells such as macrophages.[34] Consistently, in the present study, we measured the protein adsorption and cellular adhesion at 2 to 6 h and cell proliferation at 12 h to 7 days of macrophages on the different titanium surfaces to mimic the reaction *in vivo*. The results demonstrated that the hydrogel-modified titanium surface exhibited improved protein adsorption compared with the Ti-PDA and control Ti groups. As reported by Santoveña *et al.*, temperature-responsive PLGA-PEG-PLGA gels containing BMP-2 copolymers exhibited good cytocompatibility and remarkable bioadhesion.[35] Gurel Pekozer *et al.* used a biphasic scaffold consisting of a fibrous PLGA-PEG-PLGA hydrogel to load inducers of vascular endothelial growth factor-A (VEGF), which also showed good cytocompatibility both *in vitro* and *in vivo*.[36] Here, macrophage adhesion was promoted on the Ti-Gel and Ti-GL13K titanium surfaces at 4 and 6 h, suggesting that the PLGA-PEG-PLGA hydrogel with or without GL13K induced the adhesion of macrophages due to the enhanced hydrophilicity of hydrogel. The hydrophilicity of the

Table 1 Primer sequences used in this study

Gene	Forward primer sequence (5′-3′)	Reverse primer sequence (5′-3′)
IL-1β	GAAATGCCACCTTTTGACAGTG	TGGATGCTCTCATCAGGACAG
TNF-α	GCCGATGGGTTGTACCTTGT	TCTTGACGGCAGAGAGGAGG
iNOS	GAAGGGGACGAACTCAGTGG	GTGGCTCCCATGTTGCATTG
Arg-1	CAGCAGAGGAGGTGAAGAGTA	TAGTCAGTCCCTGGCTTATGG
IL-10	CTTACTGACTGGCATGAGGATCA	GCAGCTCTAGGAGCATGTGG
VEGF-A	ACTGGACCCTGGCTTTACTG	GCAGTAGCTTCGCTGGTAGA

hydrogel facilitated cellular adhesion, proliferation, and differentiation.[37] However, the results of cell proliferation showed no statistically significant differences. Thus, although the hydrogel with or without GL13K was not cytotoxic, it did not induce cell proliferation but only cell and protein adhesion at an early stage.

Immune cells such as macrophages adhere to biomaterials after the adsorption of proteins, which triggers an immune response. Inflammation and macrophage polarization affect the outcome of biomaterials.[11,38] IL-1β, TNF-α, and iNOS are the typical pro-inflammatory cytokines, whereas Arg-1, IL-10 and VEGF-A are the typical anti-inflammatory cytokines.[39] The cytokine gene and protein expression was measured in the present study. The pro-inflammatory IL-1β, TNF-α and iNOS were down-regulated on the Ti-GL13K titanium surface on days 3 and 5 at the protein level, whereas the gene expression was down-regulated on day 3, which may be explained by the earlier onset of gene expression than protein expression. The GL13K on the titanium surface may have weakened the polarization of macrophages towards M1 after three days, resulting in the reduced gene expression of pro-inflammatory cytokines. Thus, the five-day PCR results showed no difference compared with the control group. However, the protein expression by day 5 was still down-regulated in the Ti-GL13K group. Meanwhile, the anti-inflammatory cytokines Arg-1, IL-10 and VEGF-A were up-regulated partially on the Ti-GL13K titanium surface, suggesting that the macrophages were polarized to the M2 biotype. This result is consistent with other studies, such as that reported by Liu, suggesting that the synthetic hybrid peptides LB-PG and CA-PG inhibit the secretion of pro-inflammatory cytokines TNF-α and iNOS.[40] Ajish *et al.* reported that the antimicrobial peptide Lf-KR significantly inhibited the expression and production of pro-inflammatory cytokines (nitric oxide and tumor necrosis factor-α) in RAW264.7 cells.[41] The pro-inflammatory cytokines IL-1β and TNF-α up-regulate RANKL and other osteoclast-inducing factors, thus promoting osteoclast formation.[42] Meanwhile, the anti-inflammatory cytokine IL-10 inhibits osteoclasts formation by interfering with NFATc1 expression and is closely related to biomaterial-related bone regeneration.[43]

To further investigate whether the Ti-GL13K titanium surface induced macrophage polarization from the M1 to M2 phenotype, we used immunofluorescence staining and flow cytometry to measure the macrophage surface markers. The results of immunofluorescence staining, as shown in Fig. 7, demonstrated that the M1 biotype was reduced by day 3, while the M2 biotype increased by day 5. The flow cytometry analysis yielded similar results. These results support our earlier hypothesis based on the results of ELISA and PCR. Macrophages are highly plastic and polarize into various phenotypes with different functions, such as the classical activation of the pro-inflammatory M1 phenotype and bypass-activated immune regulation of the M2 phenotype, depending on the microenvironment and exposure to the surrounding environment.[44] During bone regeneration, macrophages gradually switch from the M1 to M2 phenotype, suggesting a transition from a pro-inflammatory to anti-inflammatory state, which clears local inflammation after trauma and accelerates tissue repair.[45] A higher ratio of M2/M1 phenotype on the titanium surface may prevent implant failure due to chronic inflammation, and further accelerate implant-bone osseointegration.[46]

The present study has some limitations. The oral flora is complex and the main pathogenic bacteria of peri-implantitis are *Porphyromonas gingivalis*, *Actinobacillus actinomycetemcomitans*, *Tannerella forsythia* and *Prevotella intermedi*a. However, in this study, the antibacterial performance of the modified titanium surfaces was tested using only *P gingivalis*. Thus, further follow-up animal experiments are needed to establish its effectiveness *in vivo*.

4 Experimental

4.1 Materials

Grade IV commercially pure titanium (1.0 cm × 1.0 cm in circle) was purchased from Baoji Titanium Industry Company (Shanxi, China). The antimicrobial peptide GL13K (GKIIKLKASLKLL-CONH2, MW = 1424 g mol^{-1}) was synthesized by China Peptides Co., Ltd. (Suzhou, China). The PLGA-PEG-PLGA thermosensitive hydrogel was purchased from Guangzhou Tanshui Technology Co., Ltd. (Guangzhou, China). Other materials used included dopamine (Sigma-Aldrich), LIVE/DEAD® BacLight, bacterial viability kits (Sigma-Aldrich), 4′,6′-diamidino-2-phenylindole (DAPI, Sigma-Aldrich), PE anti-mouse CD206 and CCR7 antibodies (BioLegend, USA), and anti-iNOS and anti-CD163 antibodies (HUABIO, Hanzhou, China).

4.2 Preparation of the GL13K-loaded hydrogel-coated titanium surface

Grade IV commercially pure titanium was successively immersed in acetone, anhydrous ethanol, and deionized water for ultrasonic cleaning twice, 10 min each time. The cleaned titanium served as the control group (Ti). The Ti sample was immersed in an NaOH solution at a concentration of 5 mol L^{-1} and temperature of 60 °C for 24 h. Then, the sample was transferred to deionized water at 80 °C for another 8 h after ultrasonic cleaning in deionized water. Later, the samples were immersed in a freshly prepared 2 mg mL^{-1} dopamine hydrochloride Tris–HCl buffer at room temperature for 24 h. After ultrasonic cleaning for 15 min to remove the unreacted dopamine, this titanium sample was designated as Ti-PDA. The PLGA-PEG-PLGA mixture was immersed in 0.2 mM GL13K solution in ice in a 1 : 5 ratio, followed by refrigeration at 4 °C to facilitate dissolution. Next, Ti-PDA was placed on a spin coater (KW-4B, Hengxiangtai Technology Co., Ltd., China). Then, 40 μL of gel solution was dripped on the titanium surface. The hydrogel was evenly spread on the surface of titanium with a spin coater at a speed of 6000 rpm for 15 s, to mimic a thin layer of solid gel at body temperature. The titanium surface was designated as Ti-GL13K. The single gel group (Ti-Gel) was generated using a double distilled water (ddH_2O) solution instead of the GL13K solution. All these titanium samples used were sterilized under UV for 2 h before seeding with bacteria or cells.

4.3 Surface characterization

4.3.1 Fourier-transform infrared spectroscopy (FTIR). The chemical structures of the PLGA-PEG-PLGA hydrogel, the antimicrobial peptide GL13K, and their mixtures were analyzed *via* FTIR (Bruker VERTEX 70, German) in the range of 4000–500 cm at room temperature.

4.3.2 Wettability of different modified samples. The titanium surfaces exposed to different treatments were placed in the center of the three-dimensional sample table of the instrument measuring the video optical contact angle (SINDIN SDC-100, Dongguan Shengding Precision Instrument Co., LTD). Deionized water (1 μL) was dropped perpendicular to the different modified samples. The water droplets were fully wetted on the titanium surfaces within 10 s. The system automatically fitted the image to generate two contact angles, and the average value was obtained.

4.3.3 *In vitro* degradation. The degradation of the Ti-GL13K titanium sample was evaluated based on weight loss after PBS and enzymatic hydrolysis of the samples. Firstly, the weight of the Ti-PDA titanium sample was weighed (W0). The weight of the Ti-GL13K titanium sample was denoted as W1. The titanium samples were immersed in PBS or 2 mg mL^{-1} lysozyme solution at 37 °C. During the *in vitro* degradation, the degradation solution was changed every two days. The titanium samples were removed on days 1, 3, 5, 7, 9, 11 and 13, washed with deionized water, dried and weighed (W2). The degradation of the sample was determined using the following formula: mass remaining = (W2 − W0)/(W1 − W0) × 100%.

4.3.4 *In vitro* GL13K release assay. To characterize the profile of the antimicrobial peptide GL13K released from the hydrogel, the Ti-GL13K titanium samples were placed in a 24-well plate, with each well containing 1 mL PBS buffer. The plate was placed on a shaker at room temperature, and three duplicate wells were set. The supernatant from the 24-well plate was removed and transferred to a 1 mL EP tube on days 1, 3, 5, 7, 9,11, and 13, followed by the addition of 1 mL of fresh PBS buffer to the original well. The concentration of GL13K in the supernatant was analyzed *via* ultraviolet spectrophotometry (SpectraMaxiD3, USA) at OD220.

4.4 Antibacterial assays

4.4.1 Bacteria culture. In this study, *P. gingivalis* ATCC 33277 was purchased from American Type Culture Collection (ATCC). *P. gingivalis* was cultured with Brain Heart Infusion (BHI) broth with 5% yeast extract, 1% hemin and 0.2% vitamin K1 at 37 °C under anaerobic conditions (10% CO_2, 10% H_2, and 80% N_2). The HBI-blood agar plates were composed of the same material. In addition to 2% agar, 5% sterile defibrillated sheep whole blood was added to the solid plates. A single colony of *P. gingivalis* obtained from HBI-blood agar plates was incubated in the broth at 37 °C anaerobically for another 6 h to reach the logarithmic growth phase. The *P. gingivalis* was diluted to 1 × 10^7 cells per mL and used in the following experiments.

4.4.2 Extraction medium of different titanium surfaces. The different titanium samples were placed in a 24-well plate with 0.5 mL BHI broth. The BHI broth containing GL13K was collected. Fresh 0.5 mL BHI broth was added to the 24-well plate on days 1, 3 and 5.

4.4.3 Bacterial proliferation. The different titanium samples were placed in a 24-well plate, and 1 mL of diluted *P. gingivalis* was added to each well and cultured anaerobically at 37 °C for 12 h, 24 h and 72 h. A 200 μL aliquot of bacterial liquid from 4 different wells was added to the 96-well plate and the OD value (= 600 nm) of the suspension in each well was measured on a microplate reader (SpectraMaxiD3, USA). Aliquots of *P. gingivalis* (20 μL) and extraction BHI broth (180 μL) under different extraction times were added to the 96-well plate and cultured anaerobically at 37 °C for 24 h. The OD values were also measured on a microplate reader.

4.4.4 CFU counting assay. The different titanium samples were placed in a 24-well plate and 1 mL of diluted *P. gingivalis* was added to each well and cultured anaerobically at 37 °C for 12 h, 24 h and 72 h. Next, 20 μL of *P. gingivalis* and 180 μL of the extraction BHI broth at different extraction times were added to the 96-well plate and cultured anaerobically at 37 °C for 24 h. The bacterial liquid of each sample was diluted 10^4-fold by PBS, and 10 μL of the above-mentioned microbial PBS mixture was re-incubated on HBI-blood agar plates to determine the CFUs. After 5 days of anaerobic incubation anaerobically at 37 °C, the surviving CFUs were counted.

4.4.5 Live/dead bacterial staining. The different titanium samples were placed in a 24-well plate and 1 mL of diluted *P. gingivalis* was added to each well and cultured anaerobically at 37 °C for 72 h. A biofilm exposed on different titanium surfaces was stained with the LIVE/DEAD BacLight™ Bacterial Viability Kit (Invitrogen, Thermo Fisher Scientific Inc., Shanghai, China) to determine the viability of the bacterial components in the biofilm. Bacteria with intact cell membranes can only be stained green by SYTO-9, while bacteria killed because of cell membrane destruction is stained red by propidium iodide. A confocal scanning laser microscope (Carl Zeiss AG, Oberkochen, China) was used to observe the biofilm staining at 20× magnification. The excitation wavelength of SYTO-9 is 488 nm, while that of propidium iodide is 568 nm.

4.4.6 Bacteriostasis circles. 100 μL of diluted *P. gingivalis* suspension was dropped on the HBI-blood agar plates and the bacterial solution was spread evenly with an "L"-shaped glass coating rod. Then, four different titanium samples were placed upside down on the HBI-blood agar medium and incubated anaerobically at 37 °C for 1 week.

4.5 Cytocompatibility

4.5.1 Cell culture. Macrophages (RAW 264.7 cells are a murine leukemic monocyte cell line) were purchased from ATCC and cultured in Dulbecco's modified Eagle's medium (DMEM) (HyClone, USA) supplemented with 1% penicillin–streptomycin (100×, Beyotime, China) and 10% fetal bovine serum (HyClone, USA) at 37 °C. The medium was changed every 3 days. The cells were routinely sub-cultured on reaching approximately 80% confluency. Only early passages (3 to 4) were employed in this study.

4.5.2 Protein adsorption assay. Different titanium samples were placed in a 24-well plate. To each well, 1 mL DMED-high glucose containing 10% fetal bovine serum was added, followed by incubation at 37 °C for 2, 4 and 6 h, respectively. The titanium samples were gently rinsed 3 times with PBS and transferred to new 24-well plates. Each well was treated with 20 μL of sodium dodecyl sulfate (SDS, 2 wt%) and incubated for 1 h at room temperature. Protein concentrations were determined *via* the MicroBCA protein assay (Pierce, Rockford, IL, USA), according to the manufacturer's instructions.

4.5.3 Cell adhesion. Different titanium samples were placed in a 24-well plate and RAW264.7 cells were seeded on the samples at a density of 5×10^4 cells per well. After culturing for 2, 4, and 6 h, the titanium samples were gently rinsed with PBS three times and transferred to a new 24-well plate. The cells adhering to the different titanium surfaces were fixed with 4% paraformaldehyde solution for 10 min, and then rinsed with PBS 3 times, followed by staining with 4,6-diamidino-2-phenylindole (DAPI; Sigma-Aldrich) for 3 min. The cells in each sample were counted from five random fields using a fluorescence microscope.

4.5.4 Cell proliferation. Different titanium samples were placed in a 24-well plate and RAW264.7 cells were seeded on the samples at a density of 2×10^4 cells per well and cultured for 12 h, 1 day, 3 days, 5 days, and 7 days. After each culture period, the titanium samples were washed with PBS and moved to new plates. Next, 500 mL of fresh culture medium and 50 mL of Cell Counting Kit-8 (CCK-8; Beyotime, Shanghai, China) solution were added to each well and incubated at 37 °C for another 2 h. The optical absorbance of the solution was determined using a microplate reader (SpectraMaxiD3, USA) at a wavelength of 450 nm.

4.6 Macrophage polarization assay

4.6.1 Cytokine analysis. The extracellular pro-inflammatory and anti-inflammatory cytokines were measured by ELISA (Animalunion Biotechnology Co., Ltd. China). Four different titanium samples were placed on a 24-well plate, followed by the addition of 500 μL RAW264.7 cells (1×10^5 cells per mL) to each well, and cultured for 3 to 5 days. Next, the cell culture supernatant in the 24-well plate was removed. The experimental steps were completed according to the ELISA kit instructions to measure the pro-inflammatory cytokines IL-1β, TNF-α and iNOS and anti-inflammatory cytokines VEGF-A, IL-10, and Arg. Briefly, 50 μL of cell supernatant was added to 96-well plates, which were coated with anti-mouse monoclonal antibodies for each target. The cytokines were identified with the antibodies in each well during incubation for 40 min at room temperature. The unbound materials were washed, followed by the addition of 3,3′,5,5′-tetramethylbenzidine (TMB) substrate solution. The reaction was stopped by adding 100 μL of stop solution, and the plates were read at 450 nm in a microplate reader (iMark, Bio-Rad, USA). The concentration of cytokines in the supernatant was calculated according to the standard curve and presented as picograms per milliliter (Arg in nanograms per milliliter).

4.6.2 Gene expression profiling. The gene expression of the pro-inflammatory cytokines IL-1β, TNF-α and iNOS and anti-inflammatory cytokine VEGF-A, IL-10, and Arg was measured by qRT-TCR. The total RNA was extracted using the conventional method after culturing for 3 and 5 days. cDNA was synthesized using a reverse transcription kit and sequenced after determining the RNA purity and concentration. The primer sequences (listed in Table 1) were designed by the SunYa Biological Engineering (Fuzhou) Co., Ltd. The PCR cycling conditions were initial denaturation step of 45 cycles at 95 °C for 30 s, followed by 40 cycles of denaturation at 95 °C for 5 s, and annealing at 60 °C for 30 s. Finally, the relative expression of each gene was determined using the $2^{-\Delta\Delta Ct}$ method.

4.6.3 Flow cytometry. The macrophage surface markers CCR7 (M1) and CD206 (M2) were detected by flow cytometry to evaluate the different phenotypes. RAW264.7 cells (4×10^5 cells per mL) were seeded on the different titanium samples in 24-well plates and incubated for 3 days for testing CCR7 and 5 days for CD206. The macrophages were collected from the titanium samples *via* digestion, followed by centrifugation. The cells were labeled with PE anti-mouse CD206 (Elabscience, China) and CCR7 antibodies (BioLegend, USA), according to the manufacturer's instructions. Subsequently, the cells were analysed *via* flow cytometry (FACSCalibur, BD Bioscience, USA). Data analysis was performed using the FlowJo software (Version 7.6.1, Treestar, USA).

4.6.4 Cytoimmunofluorescence staining. The macrophage surface markers iNOS (M1) and CD163 (M2) were labeled with the corresponding antibody to evaluate the different phenotypes. RAW264.7 cells (1×10^4 cells per mL) were seeded on different titanium samples in 24-well plates and incubated for 3 days for testing iNOS and 5 days for CD163. After incubation, the cells were rinsed with PBS and fixed in 4% paraformaldehyde for 20 min, and then immersed in 0.1% Triton X-100 for 10 min, followed by blocking with 3% bovine serum albumin (BSA) for 1.5 h. Subsequently, the cells were incubated with the anti-iNOS antibody (HUABIO, Hanzhou, China) or anti-CD163 antibody (HUABIO, Hanzhou, China) for 24 h. 4′,6-Diamidino-2-phenylindole (DAPI) (Solarbio, Beijing, China) was used to tag the nuclei. Inverted fluorescence microscopy was used to visualize all the samples. The fluorescence images were merged and the fluorescence intensities were quantitatively analyzed using the Image-Pro Plus 5.0 software.

4.7 Statistical analyses

All data were analysed using the SPSS software V.17.0. The mean and standard deviation were recorded and analysed *via* one-way analysis of variance (ANOVA). Multigroup comparisons of means were carried out by one-way analysis followed by Tukey's honest significant difference (HSD) post hoc test. The difference of $p < 0.05$ was considered statistically significant.

5 Conclusion

A thermosensitive PLGA-PEG-PLGA hydrogel release system containing the antimicrobial peptide GL13K was successfully

fabricated on a titanium surface using dopamine. The release persisted for 2 weeks. The modified titanium surface had a significant inhibitory effect on *P.g* in contact with its surface, as well as an inhibitory effect on *P.g* in the surrounding environment by releasing the GL13K antimicrobial peptide. Further, the modified titanium surface decreased the expression of pro-inflammatory IL-1β, TNF-α and iNOS and increased the levels of anti-inflammatory cytokines Arg-1, IL-10 and VEGF-A. It also promoted the polarization of macrophages from the M1 to M2 phenotype, which may help to create a favourable niche for bone formation under infective conditions.

Author contributions

Lin Zhou contributed to operation of the material preparation, antibacterial assays and drafting article. Yifeng Xing contributed to operation of Macrophage polarization assay. Yanjin Ou contributed to operation of the cytocompatibility of material. Jiamin Ding contributed to date collection and drafting article. Yu Han contributed to date analysis. Dong Lin contributed to date collection. Jiang Chen contributed to drafting article. All authors read and approved the final manuscript.

Conflicts of interest

The authors declare that they have no competing interests.

Acknowledgements

This work was supported by Natural Science Foundation of Fujian Province (2022J01768), Setting Foundation of Fujian Medical University (2021QH1132) and Joint Fund Project for Science and Technology innovation of Fujian Province (2019Y9031).

References

1 H. S. Alghamdi and J. A. Jansen, The development and future of dental implants, *Dent. Mater. J.*, 2020, **39**(2), 167–172.
2 J. A. López-López, R. L. Humphriss, A. D. Beswick, *et al.*, Choice of implant combinations in total hip replacement: systematic review and network meta-analysis, *Bmj*, 2017, **359**, j4651.
3 R. Trindade, T. Albrektsson, P. Tengvall, *et al.*, Foreign Body Reaction to Biomaterials: On Mechanisms for Buildup and Breakdown of Osseointegration, *Clin. Implant Dent. Relat. Res.*, 2016, **18**(1), 192–203.
4 L. Chen, D. Wang, J. Qiu, *et al.*, Synergistic effects of immunoregulation and osteoinduction of ds-block elements on titanium surface, *Bioact. Mater.*, 2021, **6**(1), 191–207.
5 S. Franz, S. Rammelt, D. Scharnweber, *et al.*, Immune responses to implants - a review of the implications for the design of immunomodulatory biomaterials, *Biomaterials*, 2011, **32**(28), 6692–6709.
6 J. O. Abaricia, A. H. Shah, M. Chaubal, *et al.*, Wnt signaling modulates macrophage polarization and is regulated by biomaterial surface properties, *Biomaterials*, 2020, **243**, 119920.
7 J. Kzhyshkowska, A. Gudima, V. Riabov, *et al.*, Macrophage responses to implants: prospects for personalized medicine, *J. Leukocyte Biol.*, 2015, **98**(6), 953–962.
8 G. P. Garlet and W. V. Giannobile, Macrophages: The Bridge between Inflammation Resolution and Tissue Repair?, *J. Dent. Res.*, 2018, **97**(10), 1079–1081.
9 E. Calciolari, S. Hamlet, S. Ivanovski, *et al.*, Pro-osteogenic properties of hydrophilic and hydrophobic titanium surfaces: Crosstalk between signalling pathways in in vivo models, *J. Periodontal Res.*, 2018, **53**(4), 598–609.
10 R. C. Costa, B. E. Nagay, M. Bertolini, *et al.*, Fitting pieces into the puzzle: The impact of titanium-based dental implant surface modifications on bacterial accumulation and polymicrobial infections, *Adv. Colloid Interface Sci.*, 2021, **298**, 102551.
11 E. Lebaudy, S. Fournel, P. Lavalle, *et al.*, Recent Advances in Antiinflammatory Material Design, *Adv. Healthcare Mater.*, 2021, **10**(1), e2001373.
12 J. A. Lemire, J. J. Harrison and R. J. Turner, Antimicrobial activity of metals: mechanisms, molecular targets and applications, *Nat. Rev. Microbiol.*, 2013, **11**(6), 371–384.
13 L. Damiati, M. G. Eales, A. H. Nobbs, *et al.*, Impact of surface topography and coating on osteogenesis and bacterial attachment on titanium implants, *J. Tissue Eng.*, 2018, **9**, 2041731418790694.
14 L. Zhou, Y. Lai, W. Huang, *et al.*, Biofunctionalization of microgroove titanium surfaces with an antimicrobial peptide to enhance their bactericidal activity and cytocompatibility, *Colloids Surf., B*, 2015, **128**, 552–560.
15 L. Zhou, Z. Lin, J. Ding, *et al.*, Inflammatory and biocompatibility evaluation of antimicrobial peptide GL13K immobilized onto titanium by silanization, *Colloids Surf., B*, 2017, **160**, 581–588.
16 M. L. Mather and P. E. Tomlins, Hydrogels in regenerative medicine: towards understanding structure-function relationships, *Regener. Med.*, 2010, **5**(5), 809–821.
17 D. Seliktar, Designing cell-compatible hydrogels for biomedical applications, *Science*, 2012, **336**(6085), 1124–1128.
18 L. Vojtova, L. Michlovska, K. Valova, *et al.*, The Effect of the Thermosensitive Biodegradable PLGA-PEG-PLGA Copolymer on the Rheological, Structural and Mechanical Properties of Thixotropic Self-Hardening Tricalcium Phosphate Cement, *Int. J. Mol. Sci.*, 2019, **20**(2), 391–412.
19 Y. Zhang, T. Yu, L. Peng, *et al.*, Advancements in Hydrogel-Based Drug Sustained Release Systems for Bone Tissue Engineering, *Front. Pharmacol.*, 2020, **11**, 622.
20 P. M. Mountziaris, P. P. Spicer, F. K. Kasper, *et al.*, Harnessing and modulating inflammation in strategies for bone regeneration, *Tissue Eng., Part B*, 2011, **17**(6), 393–402.
21 S. Kreve and A. Cândido Dos Reis, Influence of the electrostatic condition of the titanium surface on bacterial adhesion: A systematic review, *J. Prosthet. Dent.*, 2021, **125**(3), 416–420.

22 Y. Li, R. Chen, F. Wang, *et al.*, Antimicrobial peptide GL13K immobilized onto SLA-treated titanium by silanization: antibacterial effect against methicillin-resistant Staphylococcus aureus (MRSA), *RSC Adv.*, 2022, **12**(11), 6918–6929.

23 Z. Jing, R. Ni, J. Wang, *et al.*, Practical strategy to construct anti-osteosarcoma bone substitutes by loading cisplatin into 3D-printed titanium alloy implants using a thermosensitive hydrogel, *Bioact. Mater.*, 2021, **6**(12), 4542–4557.

24 P. Sahrmann, F. Gilli, D. B. Wiedemeier, *et al.*, The Microbiome of Peri-Implantitis: A Systematic Review and Meta-Analysis, *Microorganisms*, 2020, **8**(5), 661–686.

25 F. Hizal, N. Rungraeng, J. Lee, *et al.*, Nanoengineered Superhydrophobic Surfaces of Aluminum with Extremely Low Bacterial Adhesivity, *ACS Appl. Mater. Interfaces*, 2017, **9**(13), 12118–12129.

26 P. Bastos, F. Trindade, J. da Costa, *et al.*, Human Antimicrobial Peptides in Bodily Fluids: Current Knowledge and Therapeutic Perspectives in the Postantibiotic Era, *Med. Res. Rev.*, 2018, **38**(1), 101–146.

27 F. Savini, M. R. Loffredo, C. Troiano, *et al.*, Binding of an antimicrobial peptide to bacterial cells: Interaction with different species, strains and cellular components, *Biochim. Biophys. Acta, Biomembr.*, 2020, **1862**(8), 183291.

28 Y. Yan, Y. Li, Z. Zhang, *et al.*, Advances of peptides for antibacterial applications, *Colloids Surf., B*, 2021, **202**, 111682.

29 M. Magana, M. Pushpanathan, A. L. Santos, *et al.*, The value of antimicrobial peptides in the age of resistance, *Lancet Infect. Dis.*, 2020, **20**(9), e216–e230.

30 J. S. Dhaliwal, N. A. Abd Rahman, L. C. Ming, *et al.*, Microbial Biofilm Decontamination on Dental Implant Surfaces: A Mini Review, *Front. Cell. Infect. Microbiol.*, 2021, **11**, 736186.

31 S. Ferraris and S. Spriano, Antibacterial titanium surfaces for medical implants, *Mater. Sci. Eng., C*, 2016, **61**, 965–978.

32 S. Liu, Q. Wang, W. Liu, *et al.*, Multi-scale hybrid modified coatings on titanium implants for non-cytotoxicity and antibacterial properties, *Nanoscale*, 2021, **13**(23), 10587–10599.

33 K. S. J. Yang and L. Wang, Bacterial anti-adhesion surface design: Surface patterning, roughness and wettability: A review, *J. Mater. Sci. Technol.*, 2022, **99**(4), 19.

34 V. Ballotta, A. Driessen-Mol, C. V. Bouten, *et al.*, Strain-dependent modulation of macrophage polarization within scaffolds, *Biomaterials*, 2014, **35**(18), 4919–4928.

35 A. Santoveña, C. Monzón, C. Alvarez-Lorenzo, *et al.*, Structure-Performance Relationships of Temperature-Responsive PLGA-PEG-PLGA Gels for Sustained Release of Bone Morphogenetic Protein-2, *J. Pharm. Sci.*, 2017, **106**(11), 3353–3362.

36 G. Gurel Pekozer, N. Abay Akar, A. Cumbul, *et al.*, Investigation of Vasculogenesis Inducing Biphasic Scaffolds for Bone Tissue Engineering, *ACS Biomater. Sci. Eng.*, 2021, **7**(4), 1526–1538.

37 S. Yue, H. He, B. Li, *et al.*, Hydrogel as a Biomaterial for Bone Tissue Engineering: A Review, *.Nanomaterials (Basel)*, 2020, **10**(8), 1511–1535.

38 M. Pitchai, D. Ipe, S. Tadakamadla, *et al.*, Titanium Implant Surface Effects on Adherent Macrophage Phenotype: A Systematic Review, *Materials*, 2022, **15**(20), 7314–7334.

39 P. M. Mountziaris and A. G. Mikos, Modulation of the inflammatory response for enhanced bone tissue regeneration, *Tissue Eng., Part B*, 2008, **14**(2), 179–186.

40 Y. Liu, X. Xia, L. Xu, *et al.*, Design of hybrid β-hairpin peptides with enhanced cell specificity and potent anti-inflammatory activity, *Biomaterials*, 2013, **34**(1), 237–250.

41 C. Ajish, S. Yang, S. D. Kumar, *et al.*, A novel hybrid peptide composed of LfcinB6 and KR-12-a4 with enhanced antimicrobial, anti-inflammatory and anti-biofilm activities, *Sci. Rep.*, 2022, **12**(1), 4365.

42 S. Wei, H. Kitaura, P. Zhou, *et al.*, IL-1 mediates TNF-induced osteoclastogenesis, *J. Clin. Invest.*, 2005, **115**(2), 282–290.

43 K. Fujioka, T. Kishida, A. Ejima, *et al.*, Inhibition of osteoclastogenesis by osteoblast-like cells genetically engineered to produce interleukin-10, *Biochem. Biophys. Res. Commun.*, 2015, **456**(3), 785–791.

44 H. Zhang, X. Wu, G. Wang, *et al.*, Macrophage polarization, inflammatory signaling, and NF-κB activation in response to chemically modified titanium surfaces, *Colloids Surf., B*, 2018, **166**, 269–276.

45 A. J. Rao, E. Gibon, T. Ma, *et al.*, Revision joint replacement, wear particles, and macrophage polarization, *Acta Biomater.*, 2012, **8**(7), 2815–2823.

46 Y. Wang, H. Qi, R. J. Miron, *et al.*, Modulating macrophage polarization on titanium implant surface by poly(dopamine)-assisted immobilization of IL4, *Clin. Implant Dent. Relat. Res.*, 2019, **21**(5), 977–986.